EPJ Appl. Metamat. **9**, 17 (2022)

https://doi.org/10.1051/epjam/2022015

EPJ Applied Metamaterials

Available online at:
epjam.edp-open.org

Metamaterials for Novel Wave Phenomena in Microwaves, Optics, and Mechanics

RESEARCH ARTICLE OPEN ACCESS

On the role of spatial dispersion in boundary conditions for perfect non-specular reflection

Cristina Yepes[1,*], Stefano Maci[1], Sergei A. Tretyakov[2], and Enrica Martini[1]

[1] Department of Information Engineering and Mathematics, University of Siena, Siena, Italy
[2] Department of Electronics and Nanoengineering, Aalto University, Espoo, Finland

Received: 31 October 2021 / Accepted: 8 May 2022

Abstract. Exact solutions for perfect anomalous reflection through metasurfaces have been recently developed in terms of both ideal nondispersive impenetrable boundary conditions (BCs) and penetrable BCs on top of a grounded slab. The second model is more accurate for the description of metasurfaces realized in PCB technology. Focusing on this particular class of metasurfaces, this paper investigates the connection between the two solutions, with the aim to clarify the role of spatial dispersion. It is shown that the two solutions can be related through an equivalent transmission network where transmission lines with different wavenumbers are associated to the incident and reflected waves. Finally, numerical analyses are carried out to assess the impact of neglecting spatial dispersion, as it is done in designs based on a linear phase gradient of the *local* reflection coefficient.

Keywords: Metasurface / anomalous reflection / modulated surface impedance / penetrable impedance boundary condition

1 Introduction

Sixth-generation (6G) wireless communication systems are expected to be revolutionary, including applications like data driven, instantaneous, ultra-massive, and ubiquitous wireless connectivity, as well as connected intelligence. In this context, reconfigurable intelligent surfaces (RISs) [1,2] are in the spotlight, due to their potential to enhance the capacity and coverage of wireless networks through a smart reconfiguration of the wireless propagation environment. These surfaces are attractive not only for their potential, but also for their ability to be deployed on various structures such as building facades, indoor walls, aerial platforms, etc.

Metasurfaces (MTSs) are widely used to shape the refracted and reflected wavefronts to effectively control the phase, amplitude, and polarization of the field [3–5], and therefore represent a key component for the design of RISs. In particular, in order to control the propagation environment, it is crucial to have MTSs able to reflect an impinging wave in a non-specular direction, or, in other words, capable to achieve an "anomalous reflection". The possibility to achieve this effect was first illustrated introducing the reflectarray technique and, later, the generalized reflection law [6], which provided guidelines to design passive phase-gradient metasurfaces for anomalous reflection. According to this approach, the MTS is designed so as to offer to the impinging wave a local reflection coefficient whose phase is linearly varied to create the desired reflected wavefront. This means that only the transverse wavenumber of the impinging wave is considered in the definition of the reflection coefficient, even if the desired reflected wave has a different normal wavenumber, and, hence, a different transverse impedance. This design approach fails to properly account for spatial dispersion, and it is therefore inherently inaccurate. This can be seen from the fact that it does not guarantee power conservation via impedance matching with the surrounding medium. In practice, this translates in the appearance of spurious reflected lobes in the scattering pattern. The only case in which the local design based on the generalized reflection law leads to an exact solution is the case of retroreflection, where the incident and the reflected wave are characterized by the same transverse impedance.

Efforts to reduce the power lost in spurious reflected beams have been proposed in the literature, using homogenized impedance layers [7,8] or properly designed individual scatterers distributions [9]. These solutions achieve better results than the ones obtained using the phase-gradient principle by suppressing the undesired diffraction orders in the visible region, while allowing the presence of surface waves.

* e-mail: cristinayepes@ieee.org

An exact solution for perfect anomalous reflection with polarization conversion where not only the undesired diffraction orders in the visible region, but also the slow waves outside the visible region are suppressed was proposed in [10] for a nondispersive impenetrable impedance BC (IIBC). This solution rigorously satisfies power conservation by providing the right relationship between the amplitude of the incident field and the amplitude of the reflected field as a function of the incidence and reflection angles.

In principle, nondispersive anisotropic IIBCs can be realized as arrays of infinitesimal anisotropic particles. However, in practice, it is convenient to realize the MTS as a finite-thickness structure, that will inevitably exhibit some spatial dispersion. In order to account for this, in [11] a different model was proposed, based on a nondispersive penetrable IBC (PIBC) over a grounded dielectric slab, which represents a more accurate model for MTSs realized in PCB technology (the most common realization in the microwave range) [12]. This model correctly describes the spatial dispersion of the MTS, which is due to the presence of the grounded slab. Also, for this model, a solution providing perfect anomalous reflection with polarization conversion was found for any given couple of incidence and reflection angles.

This paper investigates the connection between the IIBC solution proposed in [10] and the PIBC one found in [11]. The paper is organized as follows. Section 2 introduces the impedance BCs and the relevant equivalent transmission line models. Section 3 presents the two exact solutions and discusses the connection between them. Section 4 reports some numerical results. Finally, conclusions are drawn in Section 5.

2 Impedance models for MTS description

MTSs are artificial surfaces realized by arranging small inclusions in a periodic or pseudo-periodic lattice. Their analysis can be conveniently performed by using isotropic or anisotropic impedance BCs. These conditions relate the tangential components of the average electric and magnetic fields and are obtained through a homogenization process, justified by the sub-wavelength size of the constituent unit cells.

For a modulated MTS, the definition of the effective BCs at each unit cell relies on a local periodicity assumption, i.e. it is derived by assuming the unit cell immersed in a periodic environment. For a generic MTS backed by a ground plane the BCs can be expressed in terms of an "impenetrable" equivalent tensor impedance $\underline{\underline{\mathbf{Z}}}$ which relates the average tangential electric and magnetic fields on the top interface of the MTS ($z=0$):

$$\mathbf{E}_t(z=0^+) = \underline{\underline{\mathbf{Z}}}\cdot\hat{\mathbf{z}} \times \mathbf{H}_t(z=0^+). \quad (1)$$

From here on, bold characters will denote vectors and bold characters underlined by double bars will indicate tensors. The tensor nature of the equivalent impedance accounts for possible coupling between different polarizations.

In the common case in which the MTS is realized through the PCB technology, a more accurate model can be obtained by introducing a penetrable impedance BC,

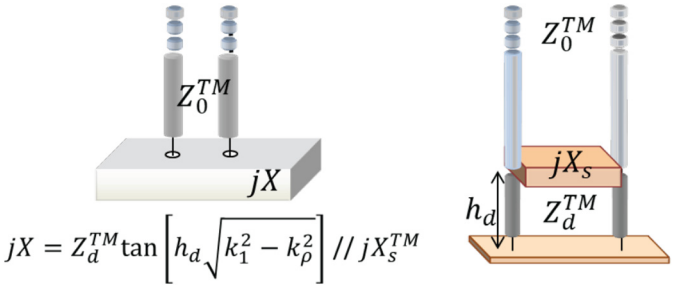

Fig. 1. Equivalent transmission line representation of a scalar metasurface using an impenetrable IBC (left) and using a penetrable IBC (right). Only the TM transmission line case is shown for the sake of simplicity.

which relates the tangential electric field to the discontinuity of the average tangential magnetic field across the metallization as follows:

$$\mathbf{E}_t(z=0) = \underline{\underline{\mathbf{Z}}}_S\cdot\hat{\mathbf{z}} \times [\mathbf{H}_t(z=0^+) - \mathbf{H}_t(z=0^-)]. \quad (2)$$

When the MTS consists of a single metallic cladding printed over a grounded slab, the relationship between the impenetrable impedance tensor $\underline{\underline{\mathbf{Z}}}$ and the penetrable one, $\underline{\underline{\mathbf{Z}}}_S$, expressed in the TM/TE reference system of the interacting wave, can be easily understood looking at the equivalent transmission-line networks in Figure 1:

$$\begin{bmatrix} Z^{ee} & Z^{eh} \\ Z^{he} & Z^{hh} \end{bmatrix}^{-1} = \begin{bmatrix} Z_S^{ee} & Z_S^{eh} \\ Z_S^{he} & Z_S^{hh} \end{bmatrix}^{-1} + \begin{bmatrix} Z_{sc}^{e} & 0 \\ 0 & Z_{sc}^{h} \end{bmatrix}^{-1} \quad (3)$$

where $Z_{sc}^{e/h}$ is the TM/TE impedance of the grounded slab.

It is noted that the impenetrable impedance model in equation (1) is more general than the PIBC one, since it can be applied to different metasurface implementations, including beds of nails and mushrooms. However, the penetrable impedance, which only represents the contribution of the patterned metallic layer, is only weakly dependent on the transverse wavenumber of the interacting fields, as opposed to the impenetrable impedance, which models the whole, finite-thickness, MTS. For this reason, the first model offers a significantly higher accuracy whenever the same BC has to be used for different transverse wavenumbers [13]. This is the case also for MTSs performing anomalous reflection, where at least two transverse wavenumbers are involved: the one of the incident wave and the one of the reflected wave.

3 Solutions for perfect anomalous reflection

It has been shown in the literature that perfect anomalous reflection without polarization conversion can only be obtained in the case of retroreflection (i.e., the impinging wave is reflected toward the same angle that it came from). On the other hand, it is possible to achieve perfect anomalous reflection in combination with polarization conversion for any given couple of incidence and reflection angles. This conclusion has been reached both for IIBC

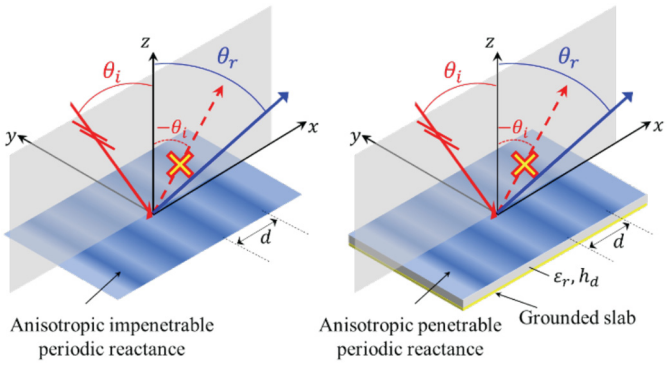

Fig. 2. Geometry for the problem of anomalous reflection. Left: impenetrable reactance. Right: penetrable reactance on a grounded dielectric slab.

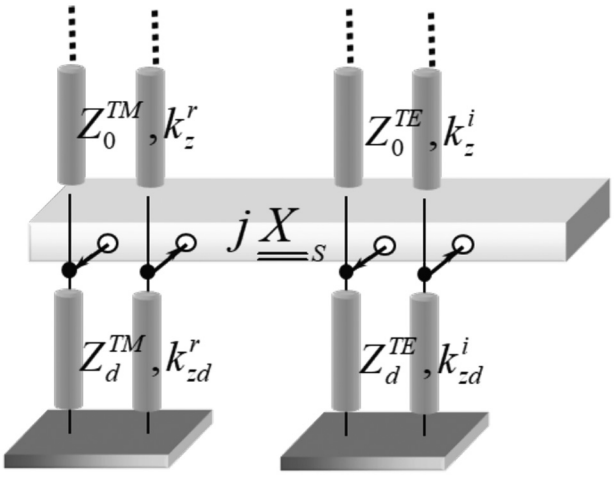

Fig. 3. Equivalent transmission line network for a TE-polarized incident wave and a TM-polarized reflected wave.

[10,14] and for PIBC [11]. The two exact solutions are summarized in the following.

The geometry for the problem is shown in Figure 2 for the two different impedance models: a MTS consisting of an impenetrable tensor reactance sheet, and a MTS made of a penetrable tensor reactance sheet on top of a grounded slab of thickness h_d and relative permittivity ε_r. For both cases, the top face of the MTS lies in the xy-plane of a Cartesian reference system, it is illuminated by a TE polarized plane wave impinging in the xz-plane at an angle θ_i, and it generates a TM-polarized reflected wave at an angle θ_r in the same plane. The MTS is modulated along x, and it is uniform along y.

The IIBC profile providing perfect anomalous reflection is provided in [10] and reads

$$\underline{\underline{Z}} = j \begin{bmatrix} \dfrac{\zeta_0}{\cos\theta_i}\cot\phi & \dfrac{\zeta_0\cos\theta_i}{\sqrt{\cos\theta_i\cos\theta_r}}\dfrac{1}{\sin\phi} \\ \dfrac{\zeta_0}{\cos\theta_i}\sqrt{\cos\theta_i\cos\theta_r}\dfrac{1}{\sin\phi} & \zeta_0\cos\theta_r\cot\phi \end{bmatrix} \tag{4}$$

where $\phi = k_0 x\,(\sin\theta_i - \sin\theta_r)$, k_0 and ζ_0 are the free space wavenumber and impedance, respectively.

The solution for the penetrable admittance providing perfect anomalous reflection has been derived in [11] and it reads

$$\underline{\underline{\mathbf{Y}}}_s = j \begin{bmatrix} -b_{sc}^{TE} + Y_0^{TE}\cot\phi & -\dfrac{\sqrt{\cos\theta_i\cos\theta_r}Y_0^{TM}}{\sin\phi} \\ -\dfrac{\sqrt{\cos\theta_i\cos\theta_r}Y_0^{TM}}{\sin\phi} & -b_{sc}^{TM} + Y_0^{TM}\cot\phi \end{bmatrix} \tag{5}$$

where

$$\begin{aligned} b_{sc}^{TE} &= -\frac{k_{zd}^i}{\zeta_0 k_0}\cot\left(k_{zd}^i h_d\right) \\ b_{sc}^{TM} &= -\frac{k_0\varepsilon_r}{\zeta_0 k_{zd}^r}\cot\left(k_{zd}^r h_d\right) \end{aligned} \tag{6}$$

with $k_{zd}^i = k_0\sqrt{\varepsilon_r - \sin^2\theta_i}$ and $k_{zd}^r = k_0\sqrt{\varepsilon_r - \sin^2\theta_r}$.

4 Connection between IIBC and PIBC solutions

The two solutions presented in the previous section support the same field configuration in the half space above the MTS since in both cases we have the same incident and reflected fields and no other modes. This implies that the ratio of the electric and magnetic fields at the top boundary of the metasurface is the same in the two cases. However, the first IBC is independent from the transverse wavenumber, while the second one is spatially dispersive due to the presence of the grounded slab. It is therefore interesting to investigate the connection between the two solutions.

To this end, we calculate the impenetrable admittance corresponding to the penetrable one reported in (5). The impenetrable impedance $\underline{\underline{Z}}$ is the parallel connection of the penetrable impedance $\underline{\underline{Z}}_s$ and the impedance of the grounded slab, which depends on the wavenumber. In this problem, two different wavenumbers are involved for the incident and the reflected waves, therefore, the definition of the impenetrable IBC appears to be non-univocal. However, it is noted that the two transverse wavenumbers are associated to different polarizations, and, hence, to two different equivalent transmission lines. We can therefore consider the equivalent transmission line represented in Figure 3, where different wavenumbers are associated to the different polarizations.

Indeed, the impenetrable IBC in [10] can be obtained from (1) only if the inclusion of the grounded slab contribution is done with two different longitudinal wavenumbers for the TE and the TM polarizations, namely, the one associated to the incidence angle for the TE polarization and the one associated to the reflection angle for the TM polarization. This leads to the unconventional equivalent transmission line shown in Figure 3, where the lines associated to the two polarizations are characterized by different propagation constants. Notice that there is no ambiguity for the cross-polar terms, since the ground plane does not couple TE and

TM modes, and therefore the off-diagonal terms of the admittance tensor representing the grounded slab contribution are zero. Hence, we can consider the tensor load $\underline{\underline{\mathbf{Y}}}_{sc} = \begin{bmatrix} jb_{sc}^{TE} & 0 \\ 0 & jb_{sc}^{TM} \end{bmatrix}$ in parallel to the penetrable impedance, leading to the impenetrable admittance $\underline{\underline{\mathbf{Y}}} = \underline{\underline{\mathbf{Y}}}_s + \underline{\underline{\mathbf{Y}}}_{sc}$:

$$\underline{\underline{\mathbf{Y}}} = j \begin{bmatrix} Y_0^{TE} \cot\phi & -\dfrac{\sqrt{\cos\theta_i \cos\theta_r} Y_0^{TM}}{\sin\phi} \\ -\dfrac{\sqrt{\cos\theta_i \cos\theta_r} Y_0^{TM}}{\sin\phi} & Y_0^{TM} \cot\phi \end{bmatrix} \quad (7)$$

which is exactly equal to the inverse of the impedance tensor in (4).

It is noted that this equivalence cannot be applied in absence of cross-polarization. The reason is that, while in the presence of cross polarization the two equivalent transmission lines associated with the incident and reflected fields are decoupled also in the presence of a linear phasing of the reflection coefficient, this is not true if the two waves have the same polarization. Hence, in this second case it is not possible to univocally define the transverse wavenumber at which the grounded slab contribution should be evaluated. The only exception is represented by the case of retroreflection, in which case the two waves are characterized by the same transverse wavenumber, and the grounded slab contribution only depends on the magnitude of the transverse wavenumber, and not on its direction. For this reason, the IIBC and the PIBC solutions are rigorously equivalent in this case, and the corresponding admittance profile read:

$$Y^{TE,TM} = -Y_0^{TE,TM} \cdot \tan\left(k_0 x \sin\theta_i\right) \quad (8)$$

$$Y_S^{TE,TM} = -Y_0^{TE,TM} \cdot \tan\left(k_0\, x \sin\theta_i\right) - b_{sc}^{TE,TM}. \quad (9)$$

As a difference from the case of arbitrary anomalous reflection with polarization conversion, the previous solutions can also be obtained by applying the generalized reflection law.

5 Numerical results

In the previous section, it has been shown that for the practical implementation of the IIBC solution for perfect anomalous reflection it is necessary to properly account for the spatial dispersion of the MTS. In order to assess the impact of this aspect, we have performed some numerical simulations to quantify how much performance degrade if spatial dispersion is not considered.

This is done by setting up a numerical procedure to analyze the scattering by a periodic MTS modeled through a PIBC on a grounded slab, illuminated by a plane wave. As shown in [13], the model based on PIBC is the most physical approach to describe PCB-based metasurfaces since it correctly describes spatial dispersion. According to it, the equivalent IIBC is given by the parallel connection of the penetrable impedance and the impedance of the grounded slab. Accordingly, any given IIBC is simulated through the equivalent PIBC, obtained by de-embedding the contribution of the grounded slab evaluated at the wavenumber of interest. The key point to set an equivalence between the IIBC solution in equation (4) and the PIBC in equation (5) is to consider the substrate admittance with different propagation constants for the TE and TM polarizations, associated to the incidence and reflection angles, respectively. This is different from the conventional way to relate IIBC and PIBC, where the same propagation constant is used for the two polarizations.

The procedure is based on the Method of Moments using Floquet Waves (FWs) as basis functions, analogous to the procedure introduced in [15] to analyze the conversion from surface waves to leaky waves. Such a procedure can be seen as a generalization of the procedure proposed by Oliner and Hessel [16] for a sinusoidally modulated scalar IIBC. A comparison between the results provided by this kind of analysis and the full-wave simulation of the patch implementation of the MTS can be found in [11] for a scattering problem and in [13] for a dispersion analysis.

The operational frequency is 10 GHz, the TE-polarized incident wave is set at $\theta_i = 0^\circ$ and the height of the dielectric is $h_d = 2$ mm. Two cases are compared: in the first one, the PIBC is the one defined by equation (5), while in the second case, it is obtained from the impenetrable IBC in equation (4) by removing the contribution of the grounded slab evaluated at the incidence angle for both the TE and the TM polarization. This is the approach that is conventionally followed for the implementation of a desired impenetrable impedance profile.

Figures 4 and 5 show the amplitude of the Floquet wave spectrum of the reflected electric field in the two cases for different TM-polarized reflected wave angles: $\theta_r = -20^\circ$ and $\theta_r = -60^\circ$. The relative permittivity of the dielectric is $\varepsilon_r = 9.8$ in Figure 4 and of $\varepsilon_r = 2.5$ in Figure 5. The reflected field is obtained as combination of the field scattered by the PIBC and the field reflected by the grounded slab. For perfect anomalous reflection, scattered field contains a contribution which exactly cancels out the specular reflection. On the other hand, cancellation is not perfect for non-exact solutions. From the results it can be appreciated that, although both the cases show the dominance of the anomalous reflected wave, the solution is exact only for the penetrable IBC, with just one reflected mode, while in the second case spurious Floquet waves are also excited, both inside (shown in Figs. 4 and 5 in yellow color) and outside the visible range (blue color bars shown in Figs. 4 and 5). This is due to the fact that spatial dispersion, intrinsic in the actual MTS implementation, is not accounted for in the derivation of equation (4).

The amplitude of the spurious waves increases when θ_r increases with respect to θ_i. The permittivity and thickness of the dielectric material also plays an important role in the amplitude of these spurious waves; for the considered thickness, spurious waves have a higher amplitude (around -8 dB) when the permittivity is smaller.

These numerical results show that the process of extracting the impedance at the incident (driving) wavenumber (local approach) is incorrect, although leading to a

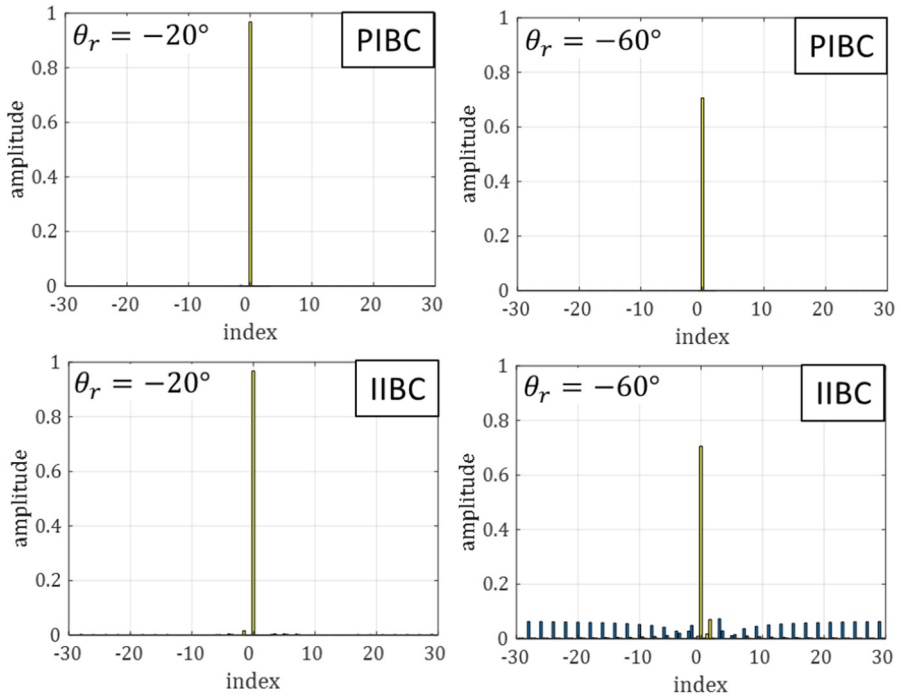

Fig. 4. Amplitude of the Floquet wave spectrum of the reflected electric field for: (top) the PIBC solution in (5) and (bottom) the PIBC obtained by removing from the IIBC in (4) the contribution of the grounded slab evaluated at the incidence wavenumber. The amplitude of the FWs is shown for an TE-polarized incident wave at $\theta_i = 0^{\circ}$ and a TM-polarized reflected wave at $\theta_r = -20^{\circ}$ and $\theta_r = -60^{\circ}$, with a permittivity of the dielectric of $\varepsilon_r = 9.8$.

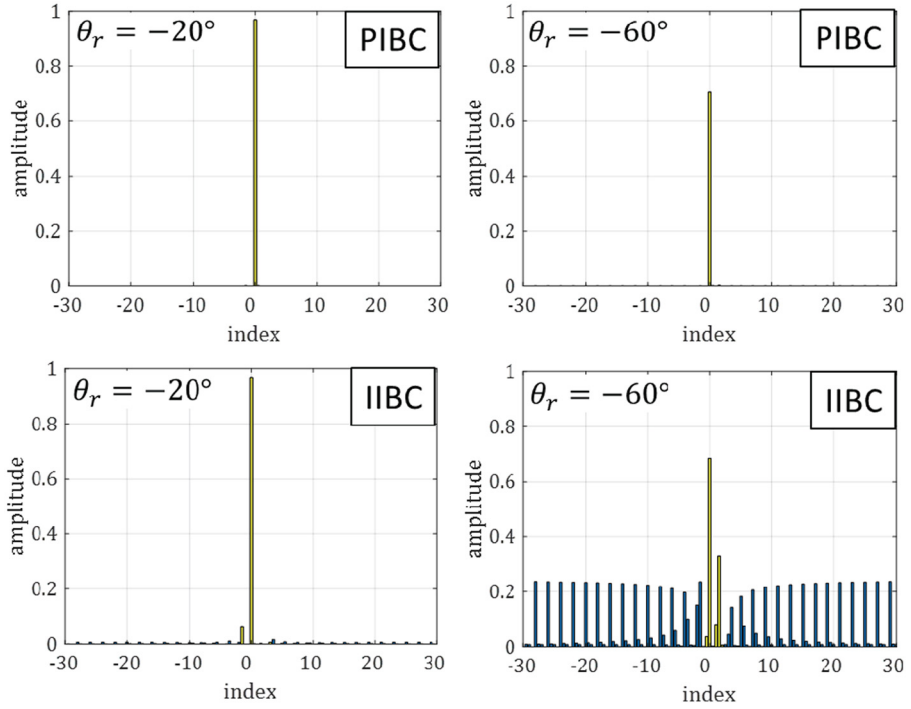

Fig. 5. Amplitude of the Floquet wave spectrum of the reflected electric field for: (top) the PIBC solution in (5) and (bottom) the PIBC obtained by removing from the IIBC in (4) the contribution of the grounded slab evaluated at the incidence wavenumber. The amplitude of the FWs is shown for an TE-polarized incident wave at $\theta_i = 0^{\circ}$ and a TM-polarized reflected wave of $\theta_r = -20^{\circ}$ and $\theta_r = -60^{\circ}$, with a permittivity of the dielectric of $\varepsilon_r = 2.5$.

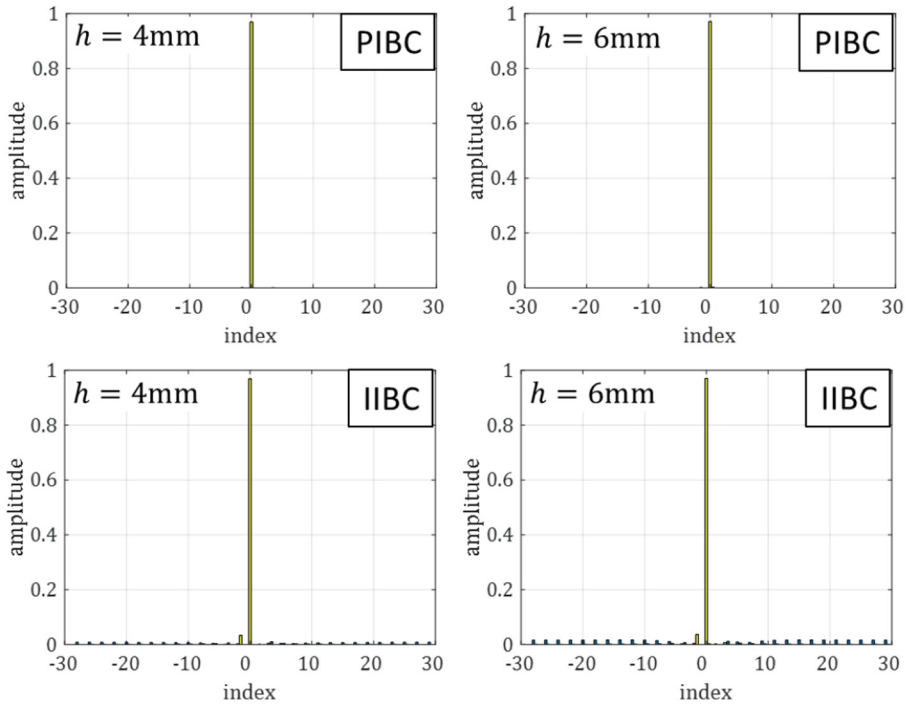

Fig. 6. Amplitude of the Floquet wave spectrum of the reflected electric field for different heights of the dielectric with a permittivity of the dielectric of $\varepsilon_r = 2.5$ for an TE-polarized incident wave at $\theta_i = 0^\circ$ and a TM-polarized reflected wave at $\theta_r = -20^\circ$ for: (top) the PIBC solution in (5) and (bottom) the PIBC obtained by removing from the IIBC in (4) the contribution of the grounded slab evaluated at the incidence wavenumber.

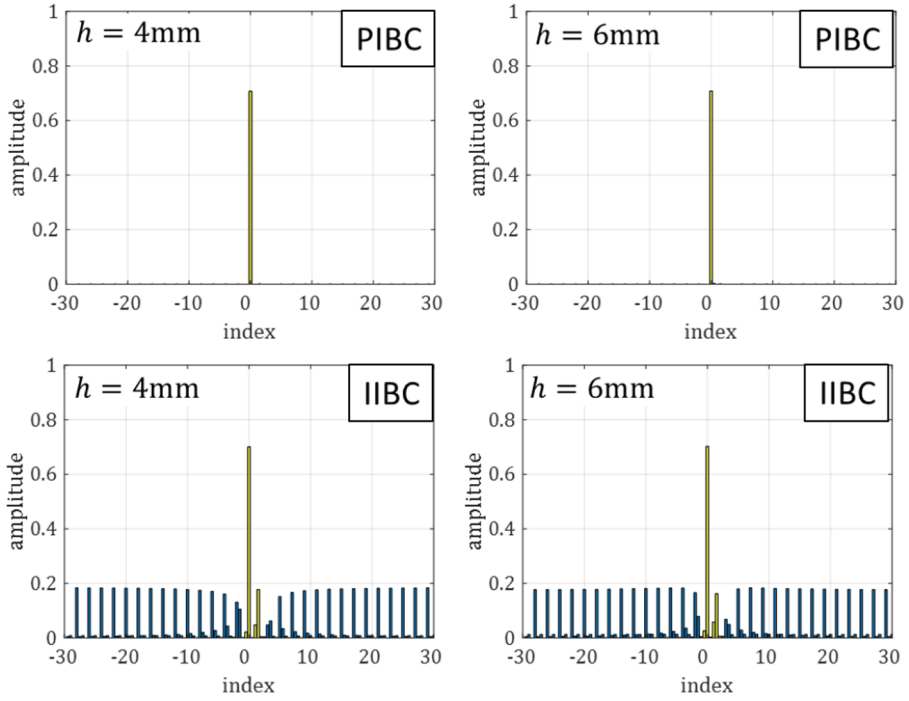

Fig. 7. Amplitude of the Floquet wave spectrum of the reflected electric field for different heights of the dielectric with a permittivity of the dielectric of $\varepsilon_r = 2.5$ for an TE-polarized incident wave at $\theta_i = 0^\circ$ and a TM-polarized reflected wave at $\theta_r = -60^\circ$ for: (top) the PIBC solution in (5) and (bottom) the PIBC obtained by removing from the IIBC in (4) the contribution of the grounded slab evaluated at the incidence wavenumber.

reasonable approximation. In fact, the exactness of the two-wave-only solution is violated by the presence of an infinite distribution of higher-order Floquet modes, arising by the improper (local) extraction of the grounded slab impedance contribution.

As mentioned before, the amplitude of the spurious waves, for the case of the IIBC, increases when θ_r increases with respect to θ_i. This is true also when the thickness of the grounded dielectric slab increases, as we can see in Figures 6 and 7, where the amplitude of the Floquet wave spectrum of the reflected electric field is calculated for the thicknesses of 4 mm and 6 mm, with the permittivity of $\varepsilon_r = 2.5$, when $|\theta_r - \theta_i| = 20°$ (see Fig. 6) and $|\theta_r - \theta_i| = 60°$ (see Fig. 7). We can appreciate that independently of the thickness of the dielectric slab the IIBC gives almost an exact solution when the difference of the incident and reflected waves directions is not big, while if the difference increases, the amplitude of the spurious in the IIBC solution is significant, no matter what the thickness of the dielectric slab is.

6 Conclusion

This paper has investigated the impact of spatial dispersion on the exact solution of the anomalous reflection problem. It has been shown that the solution found in [11] for the penetrable impedance can be related to the solution found in [10] for the impenetrable impedance by properly accounting for the spatial dispersion of the grounded slab. On the other hand, if a local approach is followed for the practical implementation of the MTS, evaluating the contribution of the grounded slab at the propagation constant associated to the incident field, spurious scattered waves are excited, whose amplitude depends on the grounded slab and on the incidence/reflection angles.

References

1. M. Di Renzo, A. Zappone, M. Debbah, M. Alouini, C. Yuen, J. De Rosny, S. Tretyakov, IEEE J. Selected Areas Commun. **38**, 2450 (2020)
2. M. Di Renzo, K. Ntontin, J. Song, F.H. Danufane, X. Qian, F. Lazarakis, J. de Rosny, D.-T. Phan-Huy, O. Simeone, R. Zhang, M. Debbah, G. Lerosey, M. Fink, S. Tretyakov, S. Shamai, IEEE Open J. Commun. Soc. **1**, 798 (2020)
3. C. Pfeiffer, A. Grbic, Phys. Rev. Lett. **110**, 197401 (2013)
4. M. Kim, A.M.H. Wong, G.V. Eleftheriades, Phys. Rev. X **4**, 041042 (2014)
5. M. Selvanayagam, G.V. Eleftheriades, Opt. Express **21**, 14409 (2013)
6. N. Yu, M. Genevet, M.A. Kats, F. Aieta, J.P. Tetienne, F. Capasso, Z. Gaburro, Science **334**, 333 (2011)
7. A. Epstein, G.V. Eleftheriades, Phys. Rev. Lett. **117**, 256103 (2016)
8. A. Díaz-Rubio, V.S. Asadchy, A. Elsakka, S.A. Tretyakov, Sci. Adv. **3**, e1602714 (2017)
9. Y. Ra'di, D.L. Sounas, A. Alù, Phys. Rev. Lett. **119**, 067404 (2017)
10. V.S. Asadchy, M. Albooyeh, S.N. Tcvetkova, A. Díaz-Rubio, Y. Ra'di, S.A. Tretyakov, Phys. Rev. B **94**, 075142 (2016)
11. C. Yepes, M. Faenzi, S. Maci, E. Martini, Appl. Phys. Lett. **118**, 231601 (2021)
12. A.M. Patel, A. Grbic, IEEE Trans. Antennas Propag. **61**, 211 (2013)
13. E. Martini, F. Caminita, S. Maci, EPJ Appl. Metamat. **7**, 12 (2020)
14. N. Mohammadi Estakhri, A. Alù, Phys. Rev. X **6**, 041008 (2016)
15. S.N. Tcvetkova, E. Martini, S.A. Tretyakov, S. Maci, IEEE Trans. Antennas Propag. **68**, 6145 (2020)
16. A. Oliner, A. Hessel, IRE Trans. Antennas Propag. **7**, 201 (1959)

Cite this article as: Cristina Yepes, Stefano Maci, Sergei A. Tretyakov, Enrica Martini, On the role of spatial dispersion in boundary conditions for perfect non-specular reflection, EPJ Appl. Metamat. **9**, 17 (2022)